Urea Induces Uniform Tin Deposition for Long Cycle-Life Tin-based Redox Flow Battery

Yang, Yang; Xiang, Yan; Yang, Yuewen; Xie, Xian; Mushtaq, Faheem; Zhang, Ruiqin; Daoud, Walid

Published in:
Advanced Functional Materials

Published: 12/08/2024

Document Version:
Final Published version, also known as Publisher's PDF, Publisher's Final version or Version of Record

Published version (DOI):
10.1002/adfm.202413685

Publication details:
Yang, Y., Xiang, Y., Yang, Y., Xie, X., Mushtaq, F., Zhang, R., & Daoud, W. (2024). Urea Induces Uniform Tin Deposition for Long Cycle-Life Tin-based Redox Flow Battery. *Advanced Functional Materials*, Article 2413685. https://doi.org/10.1002/adfm.202413685

ADVANCED FUNCTIONAL MATERIALS
www.afm-journal.de

Urea Induces Uniform Tin Deposition for Long Cycle-Life Tin-based Redox Flow Battery

Yang Yang, Yan Xiang, Yuewen Yang, Xian Xie, Faheem Mushtaq, Ruiqin Zhang, and Walid A. Daoud**

Among multivalent redox flow batteries, the Zn-based redox flow battery (RFB) has the advantages of high energy density, nontoxicity, and low cost. However, the severe dendrite issue hinders its deployment. Therefore, the Sn-based RFB is reported as a prospective alternative, particularly in alkaline systems, due to its lower redox potential and four electrons transfer in redox reactions. However, the continuous growth of Sn during charge forms large Sn bulk, which increases the risk of "dead Sn" formation. By combining experiments and theoretical calculations, urea is proposed as an electrolyte additive to regulate Sn deposition on graphite felt. This is achieved through the enhanced adsorption and robust reaction of $Sn(OH)_6^{2-}$ with graphite felt. Consequently, a more uniform morphology ensues, reducing "dead Sn" formation and thus improving the average discharge voltage and areal capacity. Moreover, the Columbic efficiency becomes more stable, extending the cycle life to over 420 h (>200 cycles) without deep discharge during cycling. This study demonstrates the role of urea in achieving high-performance Sn-I flow battery with long cycle life, paving the way for further development of metal-based hybrid RFBs.

1. Introduction

Depleting fossil energy promotes a rising demand for renewable energy, where efficient energy storage systems are crucial in the transition to renewable energy. Redox flow batteries (RFB) are considered one of the most prospective storage technologies due to its large capacity, high safety and efficiency, and long cycle life.[1] In RFBs, electrolytes serve as energy carriers are stored in two independent external storage tanks. To date, the all-vanadium RFB is the most mature energy storage technology.[2] However, the high cost and low energy density of vanadium electrolytes limit its further development.[3] Therefore, RFBs employing low-cost redox species are more promising, such as Zn-based RFB (ZRFB),[4] Fe-based RFB,[5] Sn-based RFB,[6] and redox-active organic materials-based RFB.[7] ZRFBs in neutral/mild systems are close to commercialization due to the merits of high energy density, nontoxicity, low cost, and environmental friendliness.[8] In contrast to neutral/mild systems (−0.76 V vs standard hydrogen electrode, SHE), the redox potential of ZRFB is relatively lower in alkaline systems (−1.26 V vs SHE).[9] However, severe dendrite growth in alkaline electrolytes increases the risk of short-circuiting during charging. Additionally, "dead zinc" may form during the discharge process, decreasing the battery's discharge capacity, and potentially blocking the electrolyte flow.[10]

Compared with neutral/mild Zn^{2+}/Zn (−0.76 V vs SHE), the alkaline $Sn(OH)_6^{2-}/Sn$ electrocyte has a more negative redox potential (−0.921 V vs SHE), resulting in a larger cell voltage for the Sn-I battery. Moreover, Sn can transfer four electrons ($Sn(OH)_6^{2-} \rightarrow Sn$) in alkaline systems. As shown in Figure S1a (Supporting Information), the intermediate of the Sn redox reaction in an alkaline environment is $Sn(OH)_3^-$, which is strongly reductive. The redox reactions of $Sn(OH)_6^{2-}/Sn$ are given below.[11]

$$Sn(OH)_6^{2-} + 2e^- \leftrightarrow Sn(OH)_3^- + 3OH^- \quad E = -0.91\ V\ (vs\ V_{SHE}) \tag{1}$$

$$Sn(OH)_3^- + 2e^- \leftrightarrow Sn + 3OH^- \quad E = -0.921\ V\ (vs\ V_{SHE}) \tag{2}$$

In addition, a dendrite-free Sn anode for RFB has been reported.[12] Unlike Zn, which has a preferential growth plane due to the difference in surface energy,[13] the body-centered tetragonal crystal structure of Sn enables its isotropic growth,[14] resulting in more uniform Sn deposition. Moreover, the lower Young's modulus ($E_{Sn} \approx 50$ GPa) of Sn compared to Zn ($E_{Zn} \approx 108$ GPa) reduces the risk of piercing the membrane, further extending the battery cycle life.[15] Furthermore, a Sn-modified

Y. Yang, Y. Xiang, X. Xie, F. Mushtaq, W. A. Daoud
Department of Mechanical Engineering
City University of Hong Kong
Kowloon Tong, Hong Kong
E-mail: wdaoud@cityu.edu.hk

Y. Yang, R. Zhang
Department of Physics
City University of Hong Kong
Kowloon Tong, Hong Kong
E-mail: aprqz@cityu.edu.hk

The ORCID identification number(s) for the author(s) of this article can be found under https://doi.org/10.1002/adfm.202413685

DOI: 10.1002/adfm.202413685

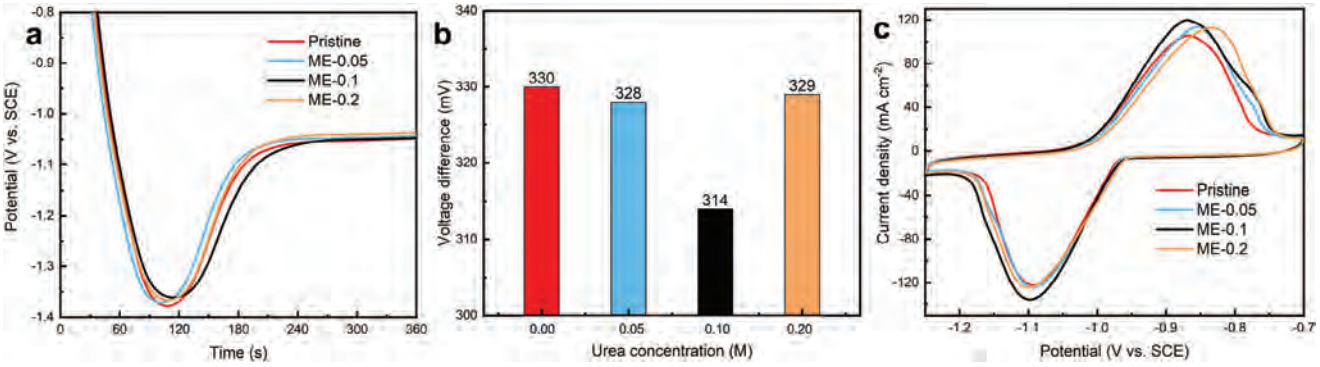

Figure 1. a) Voltage-time curve of during Sn nucleation and growth on TGF in pristine and modified electrolytes at 20 mA cm^{-2}; b) The comparison of overpotential of different samples; c) Cyclic voltammograms of $Sn(OH)_6^{2-}$/Sn redox reaction at a scan rate of 10 mV s^{-1}.

Zn anode has been shown to improve battery performance due to higher suppression of hydrogen evolution reaction (HER).[16] However, the continuous growth of bulk Sn still increases the risk of forming "dead Sn", leading to battery capacity loss. Therefore, regulating Sn deposition to enhance battery performance is vitally significant.

According to the literature, approaches to improve the electrochemical performance of RFBs are mainly focused on modifying the electrodes, electrolytes, and membranes.[17] Among them, modifying electrolytes with additives is the most facile way to regulate metal deposition via a simple and low-cost fabrication process.[18] Up to now, the modification approach of alkaline Sn-based RFB has yet to be reported. In this work, we introduced urea as a novel, low-cost, and effective additive at an optimum concentration of 0.1 M. The corresponding Sn-I RFB, as shown in Figure S1b (Supporting Information), features a cathode reaction of $6I^- \leftrightarrow 2I_3^- + 4e^-$ (E = 0.536 V vs SHE). The effect of urea on Sn-I flow battery performance is investigated through experiment and theoretical calculations, demonstrating that urea induces uniform Sn deposition on graphite fibers and suppresses the formation of "dead Sn." Consequently, the urea-modified Sn-I battery shows higher areal capacity, more stable columbic efficiency, and higher average discharge voltage and cycling stability.

2. Results and Discussion

To confirm the successful adsorption of urea on thermally-treated graphite felt (TGF), XPS wide scan spectra of TGF in the pristine electrolyte and ME-0.1 in the binding energy range of 1–1400 eV were collected as shown in Figure S2 (Supporting Information). The spectra display that the N 1s and O 1s signal of TGF with urea additive are more potent than that of pure TGF, indicating that urea containing double bond C=O and single bond -NH_2 groups can be adsorbed on TGF surface.

To investigate Sn deposition electrochemistry on TGF, **Figure 1a** shows the voltage-time curves of TGF in pristine and modified electrolytes during Sn nucleation and growth at a current density of 20 mA cm^{-2} for 6 min. At the beginning of Sn plating on TGF, the voltage decreased continuously. The voltage dip represents the Sn nucleation process, as the nucleation of a new solid phase needs to overcome an energy barrier.[19] Then, the voltage increased since subsequent atomic Sn deposition is more favorable on existing Sn nuclei due to the lower energy barrier compared to forming a new cluster of Sn atoms.[20] The voltage difference between the dip and the flat part represents Sn nucleation overpotential, which determines the difficulty of nucleation. Thus, lower nucleation overpotential indicates lower nucleation resistance and more controlled nucleation sites, contributing to regulating the subsequent Sn deposition.[21] The overpotential of different samples are compared in Figure 1b, and ME-0.1 shows the most even voltage dip and the smallest nucleation overpotential. In ME-0.2, the overpotential in the electrolyte increased again, probably due to the increased viscosity. Overall, the voltage-time results indicate that urea can lower the nucleation energy barrier to facilitate Sn formation, thus promoting subsequent Sn deposition on the TGF surface.

After depositing Sn on TGF at 20 mA cm^{-2} for 6 min, CV tests were conducted to investigate the $Sn(OH)_6^{2-}$/Sn redox couples in the pristine electrolyte, ME-0.05, ME-0.1, and ME-0.2 in the range of −0.7 to −1.25 V at a scan rate of 10 mV s^{-1}. The cyclic voltammograms are shown in Figure 1c. Compared with the pristine electrolyte, the current density increased during the reduction and oxidation processes, indicating enhanced kinetics of the redox reactions.[22] Moreover, a shoulder peak appears at ≈−0.78 V, associated with the reaction intermediates during the oxidation reaction of Sn to $Sn(OH)_6^{2-}$, which is consistent with a previous report.[12] The higher current densities of the shoulder peaks over pristine electrolyte also indicate that urea effectively promotes the intermediate reaction. On the other hand, a positive voltage shift of the first peak occurred during oxidation in ME-0.2.

To investigate the effect of urea during Sn charging, the Sn deposition morphology under a current density of 20 mA cm^{-2} at different deposition times from 5 to 25 min is compared using SEM images, as shown in **Figure 2**. The right-side images in the red dashed box show magnified images of the left-side images (a–f). The energy dispersive X-ray spectroscopy (EDS) spectra of graphite felt in ME-0.1 after charging for 6 min at 20 mA cm^{-2} is shown in Figure S3 (Supporting Information). In the pristine electrolyte, uneven deposition morphology is observed on the surface of graphite fibers after charging for 5 min (Figure 2a), with scattered small-size Sn particles and large Sn bulks. When the charging time reached 15 min, the size of Sn bulks further increased due to particle accumulation (Figure 2b). After charging for 25 min, Sn particles cannot fully cover the surface of graphite fibers due to uneven deposition and larger Sn bulk

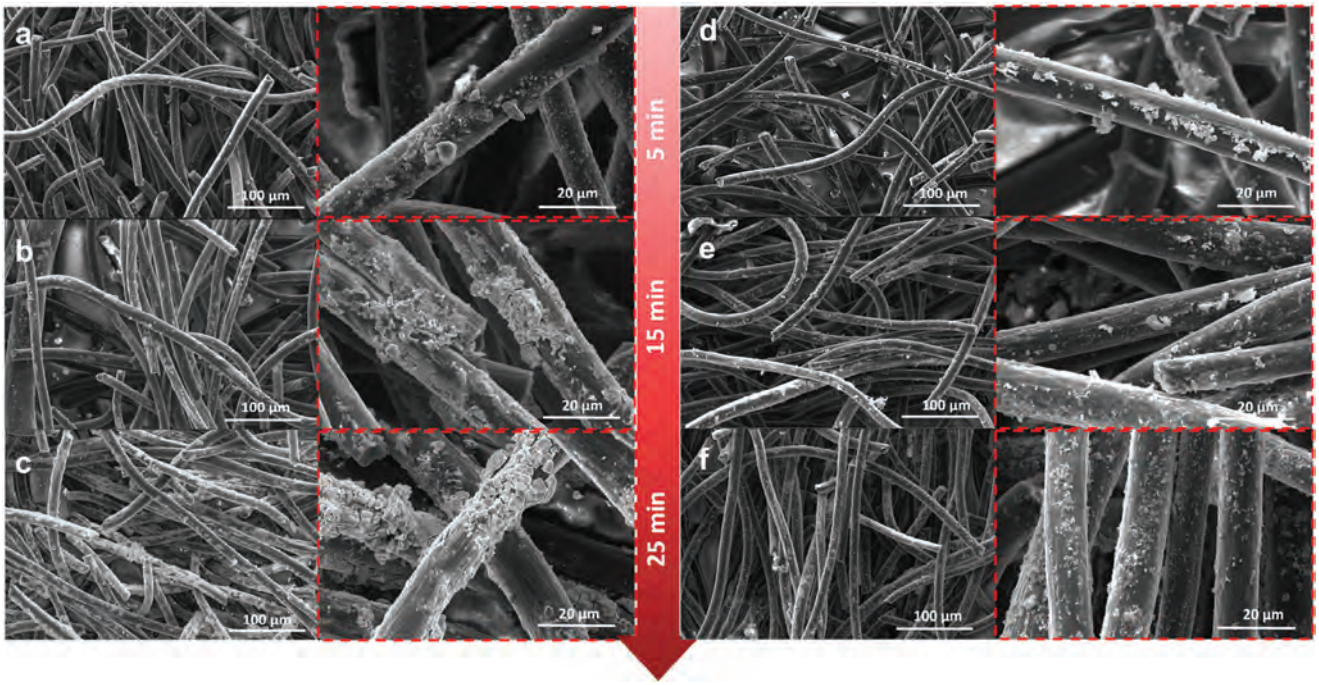

Figure 2. SEM images of Sn deposition on TGF in the pristine electrolyte a–c) and ME-0.1 d–f) at current density of 20 mA cm^{-2} at different deposition time from 5 to 25 min.

formation (Figure 2c), which increases the probability of forming "dead Sn" during discharge, thus decreasing the CE. In contrast, fewer large Sn particles were deposited between fibers and their morphology is more uniform in ME-0.1. After charging for 5 min, fine Sn particles were deposited on the fibers with wider coverage compared to the pristine electrolyte (Figure 2d). When the charging time increased to 15 min, the surface of graphite fibers was covered by more Sn particles with less large Sn particles formation (Figure 2e). When the charging time reached 25 min, a much denser Sn deposition layer ensued, covering most of the graphite fibers surface without large Sn bulks (Figure 2f), which is in sharp contrast with that in the pristine electrolyte (Figure 2c). Moreover, the optical images of "dead Sn" flowed to the negolyte tank after charging for 25 min and discharging to cutoff voltage of 0.1 V are shown in Figure S4 (Supporting Information). Compared with pristine electrolyte, there is no "dead Sn" in ME-0.1. Therefore, adsorbed urea promotes uniform Sn deposition on graphite fibers during the early stage of Sn plating, consistent with the voltage-time results. Moreover, the subsequent uniform Sn growth further reduces the risk of "dead Sn" formation.

Furthermore, to compare the Sn deposition morphology in the late stage of charging, optical images of TGF in pristine electrolyte and ME-0.1 after charging for 5 h at a current density of 10 mA cm^{-2} are compared, as shown in **Figure 3**. Noticeably, large Sn bulks formed between graphite fibers in the pristine electrolyte due to severe aggregation (Figure 3a), while in ME-0.1 (Figure 3b), a more uniform Sn deposition layer was observed. This is consistent with the SEM analysis during charging from 5 to 25 min at 20 mA cm^{-2} and further supports the role of urea in promoting uniform Sn deposition. Furthermore, the impact of urea on the morphology of Sn deposition is schematically illustrated in Figure 3c.

The successful Sn deposition and the changes of Sn microstructure and morphology on graphite fiber after charging were further confirmed through XRD analysis, as shown in **Figure 4**a. The TGF samples after charging were directly milled without washing for XRD analysis. Thus, the peaks of $K_2Sn(OH)_6$ and KOH are shown in both samples. For the TGF in ME-0.1, the intensity of the (101) peak at $2\theta^\circ \approx 32^\circ$ exhibits a significant increase, and it is much higher than the (200) peak, as shown in Figure 4b. This indicates the role of urea in regulating the growth direction of the Sn crystal structure. The (101) peak grows along an inclination rather than on the vertical plane of the (200) peak, indicating suppression of Sn growth in the vertical direction during charging, resulting in a more uniform deposition.

XPS analysis was performed to further confirm the binding energy change of each element. The deposition of Sn on TGF in the pristine electrolyte and ME-0.1 is confirmed by XPS, as shown in Figure S5 (Supporting Information). Figure 4c shows high-resolution C 1s spectra of TGF, which can be characterized by three peaks at 284.8, 285.9, and 288.3 eV, corresponding to C—C, C—N, and C═O bonds, respectively. In ME-0.1, the binding energy of C═O increased slightly, indicating amide group formation.[5b] The N 1s and O 1s spectra of urea and TGF in ME-0.1 are shown in Figure S6a,b, (Supporting Information) where it can be observed that the peaks associated with urea occurred at 399.5 and 531.3 eV. In ME-0.1, the -NH_2 peak located at 399.5 eV shifted to 399.9 eV and the −C═O peak at 531.3 eV increased to 531.7 eV. The higher binding energy indicates enhanced adsorption of urea. Furthermore, to compare the binding energy of Sn deposition in the pristine electrolyte and ME-0.1, the Sn 3d spectra are analyzed (Figure 4d), showing that all Sn 3d peaks positioned at 485.7, 487.3, 494.1, and 495.7 eV shift to higher binding

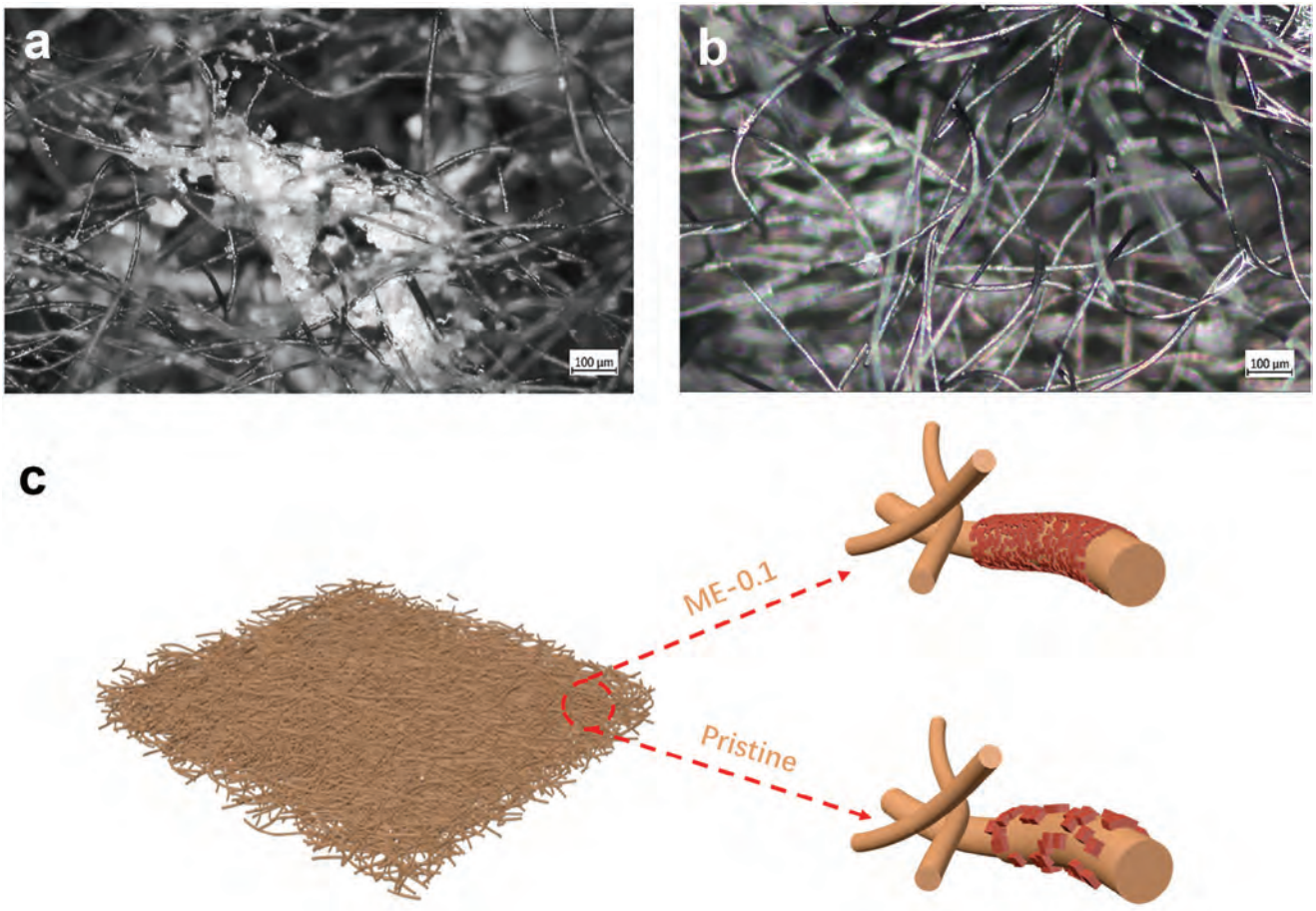

Figure 3. Optical images of Sn deposition on TGF in a) the pristine electrolyte and b) ME-0.1 after charging 5 h at a current density of 10 mA cm^{-2}; c) Schematic diagram of the Sn deposition process in the pristine electrolyte and ME-0.1.

energy of 486.2, 488.1, 494.6, and 496.5 eV, respectively, confirming the distinct adsorption between Sn and urea.

Additionally, density functional theory (DFT) calculations were performed to analyze the effects of urea on Sn deposition. According to previous studies, graphene is a good model to simulate carbon materials.[23] The structural models of TGF materials were constructed using an 8 × 8 graphene hexagonal supercell with OH adsorbed, in a lattice of a = b = 19.68 Å, c = 20.00 Å, and $\alpha = \beta = 90°$, $\gamma = 120°$ (**Figure 5**) (refer to the Supporting Information for computational details). For $Sn(OH)_6^{2-}$, the most adsorption-stable geometry was determined to involve hydrogen bonding with the OH moiety (Figure 5a-I). The small adsorption energy (ΔE_{ads}) of −0.07 eV suggests a weak interaction between $Sn(OH)_6^{2-}$ and TGF surface. The differential charge density distribution shows that $Sn(OH)_6^{2-}$ has a net charge of ≈−1.37 |e|, and donates electrons to TGF (Figure 5a-II). In contrast, the presence of urea significantly enhances the adsorption through the formation of two hydrogen bonds, resulting in an increased ΔE_{ads} of −0.56 eV (Figure 5b-I). On the other hand, urea donates electrons to TGF, but accepts electrons form $Sn(OH)_6^{2-}$, resulting in a net charge of almost zero (Figure 5b-II). Meanwhile, the ab initio molecular dynamics (AIMD) simulation confirmed the stability of this adsorption geometry (Figure S7, Supporting Information), and the density of state is shown in Figure S8 (Supporting Information). This enhancement is attributed to robust interaction between $Sn(OH)_6^{2-}$ and urea, where the ΔE_{ads} is ≈−1.32 eV (Figure 5c). Urea exhibits a preference for orienting its two H atoms toward the two O atoms of $Sn(OH)_6^{2-}$, which is fundamentally attributed to the favorable orbital matching between urea and $Sn(OH)_6^{2-}$.[24] The highest occupied molecular orbital (HOMO) of $Sn(OH)_6^{2-}$ (Figure 5d-I) reveals orbital localization on the Sn and OH bonds. Additionally, the lowest unoccupied molecular orbital (LOMO) of urea (Figure 5d-II) indicates a significant orbital distribution on NH_2 moieties, which serve as the active sites for forming hydrogen bonds, leading to a charge of −0.14 |e|. Thus, the effect of urea on improving the adsorption of $Sn(OH)_6^{2-}$ on TGF is confirmed, which promotes the deposition of Sn and reduces the risk of Sn detaching from the graphite fibers.

The rate performance of Sn-I full cell was conducted at a charge current density of 10 mA cm^{-2} for 5 h to fix the areal charge capacity (50 mAh cm^{-2}) and discharge at current densities of 10, 15, and 20 mA cm^{-2}, as shown in **Figure 6**a–c. First, each charge curve shows a steep voltage peak at the beginning of the charging process, where the voltage peak in ME-0.1 is lower, which is consistent with the voltage-time results. In Figure 6a–c,

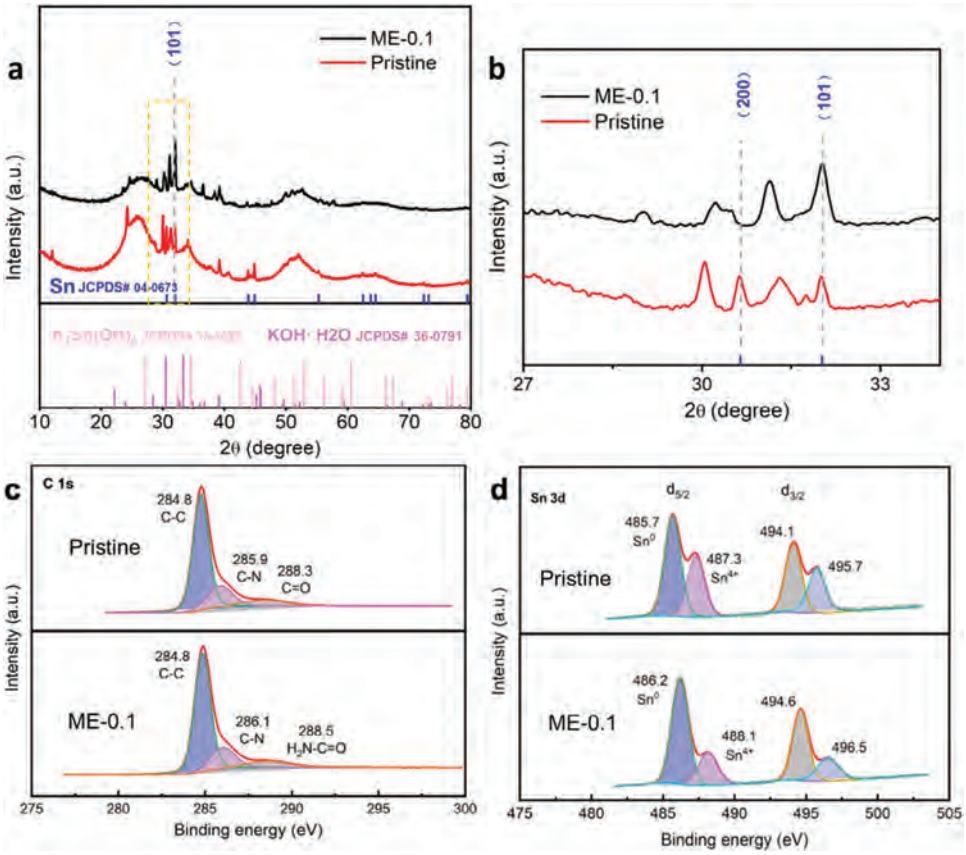

Figure 4. a) XRD pattern and b) partial angle pattern of Sn deposition on TGF in the pristine electrolyte and ME-0.1; c) C 1s XPS spectra of TGF in the pristine electrolyte and ME-0.1; d) Sn 3d XPS spectra of Sn deposition on TGF in the pristine electrolyte and ME-0.1.

compared with the pristine electrolyte, the initial discharge voltage is lower in ME-0.1 during the first voltage platform. Since Sn tends to form large bulks in the pristine electrolyte, the activity of bulk edges is higher than that in the uniform deposition layer, resulting in a higher electric field, which causes a higher discharge voltage. Thus, the lower voltage indicates the more uniform Sn deposition. Moreover, the first voltage platform was prolonged in the discharge curve of ME-0.1, indicating promotion of reaction (1), which is consistent with the CV results. Furthermore, the Sn-I full cell exhibited an areal capacity of 43.5 mAh cm^2 with an average discharge voltage of 1.05 V and CE of 87%, whereas in ME-0.1, the areal capacity, average discharge voltage, and CE reached 46.2 mAh cm^{-2}, 1.18 V and 92.4%, respectively, demonstrating improved electrochemical performance. Since the bottom of Sn bulk in the pristine electrolyte is likely dissolved during discharge, causing large Sn bulk easily to detach from graphite felt, which led to a sharp drop in capacity and less utilization of deposited Sn. While in ME-0.1, the uniform Sn deposition ensures mild stripping of Sn, leading to higher areal capacity, CE, and average discharge voltage. Figure 6b,c show a similar contrast of the discharge curves in the pristine electrolytes and ME-0.1, and the areal capacity and average discharge voltage are compared in **Table 1**, further demonstrating enhancement in ME-0.1 at different discharge current densities. The areal capacities achieved in Sn–I RFB in our work are competitive with Sn-based and most of Zn-based RFBs reported in recent literature (Table S1, Supporting Information). Furthermore, to investigate the impact of self-discharge, a standby test was conducted to study capacity retention. Figure 6d shows the discharge curves of the Sn-I flow cell using pristine electrolyte and ME-0.1 after 5 h charging at a current density of 12 mA cm^{-2} and 20 h idle period with no electrolyte flow. It can be observed that the discharge curve of full cell employing ME-0.1 prolonged the first platform, which indicates sustained promotion of the reaction. Moreover, the full cell displays an average voltage of 1.07 V and CE of 76% in the pristine electrolyte, while in ME-0.1, the average voltage and CE reach 1.19 V and 82%, respectively. The capacity decay of full cell was mainly caused by self-discharge, which occurred during the idle period. Self-discharge can be more severe owing to the uneven Sn deposition since the activity of Sn bulk edge is relatively higher than that in uniform deposition. The higher capacity retention in ME-0.1 indicates reduced self-discharge due to the more uniform Sn distribution, which is consistent with the SEM results.

The cycle performance of Sn–I full cell employing pristine electrolyte and ME-0.1 was compared at a current density of 10 mA cm^{-2}, as shown in Figure 6e. The voltage-time curve of pristine electrolyte shows a short cycle life (<50 cycles) due to the large Sn bulk formation, which blocked electrolyte flow and stopped the subsequent charge/discharge process. In comparison, the voltage-time curve demonstrates a more stable Sn plating/stripping and longer cycle life (>200 cycles at 10 mA cm^{-2} without deep discharge) in ME-0.1. In addition, to assess the

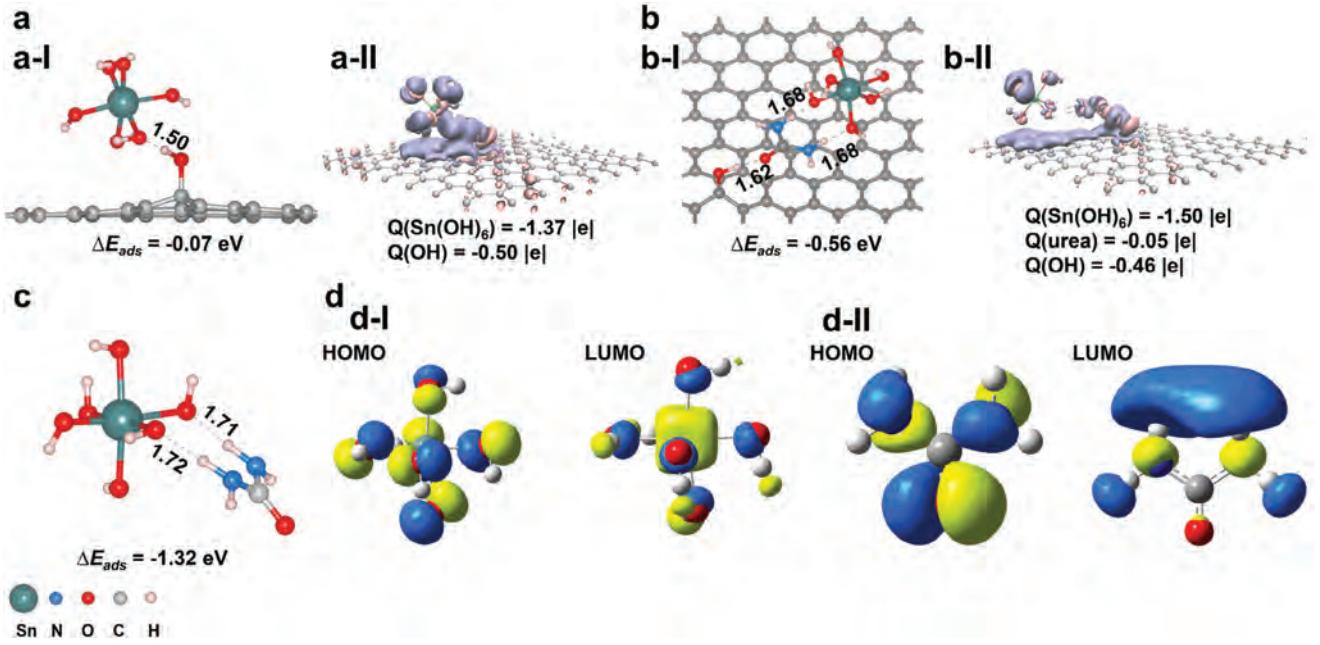

Figure 5. a,b) The optimized adsorption structures. The adsorption configuration of (a-I) isolated $Sn(OH)_6^{2-}$ with (a-II) differential charge density distribution. The adsorption configuration of (b-1) $Sn(OH)_6^{2-}$ via urea on the TGF surface with (b-II) differential charge density distribution. The Q stands for the charge (in |e|), and the isovalue was set as 0.0008 a.u (ice blue: accepting electrons, and pink: donating electrons). The key distances (unit: Å), and adsorption energies (ΔEads, unit: eV) are marked. c) The optimized geometry of $Sn(OH)_6^{2-}$hydrogen bonded to urea. d) The highest occupied molecular orbital (HOMO) and the lowest unoccupied molecular orbital (LOMO) of (d-I) $Sn(OH)_6^{2-}$ and (d-II) urea. The isovalue was set as 0.05 a.u.

stability of Sn plating/stripping behavior and reflect on the role of urea on Sn deposition, the Coulombic efficiency of Sn-I full cell was studied, as shown in Figure 6f. In the pristine electrolyte, CEs were unstable, ranging from 77.9% to 107.8%. As larger Sn bulks tend to form in the pristine electrolyte during cycling, the continuous electrolyte flow increased the possibility of Sn bulk detaching from graphite fibers, forming "dead Sn", which led to the lower and unstable CE. In contrast, CEs are more stable in ME-0.1 and decreased by only 2% after cycling for over 420 h, due to the more uniform Sn plating and stripping. Moreover, Figure S9a (Supporting Information) shows the optical images of "dead Sn" flowed to the negolyte tank after 200 cycles, where significantly higher amount of "dead Sn" was formed compared to ME-0.1 (Figure S9b, Supporting Information).

3. Conclusion

In this work, the impact of urea on Sn deposition in Sn-I flow battery was investigated. It is found that urea lowered the nucleation energy barrier and increased the kinetics of $Sn(OH)_6^{2-}$/Sn redox reactions, which facilitated Sn formation. Owing to the amide group of urea, hydrogen bonds improved the interaction with $Sn(OH)_6^{2-}$, where the adsorption of $Sn(OH)_6^{2-}$ on the graphite fiber surface was significantly enhanced, resulting in a more uniform Sn deposition morphology and suppression of "dead Sn" formation, which enhanced Sn utilization during charge and discharge. Consequently, the Sn-I flow battery shows higher areal capacity at different discharge current densities (46.2 mAh cm^{-2} at a current density of 10 mA cm^{-2}) and long cycle life with more stable CE over 420 h (>200 cycles). The results demonstrate the role of urea as a low-cost solution for high-performance Sn-I flow battery with long cycle life.

4. Experimental Section

Materials: Potassium iodide (KI, 99%) was purchased from Sinopharm Chemical Reagent Co., Ltd., Potassium tin (IV) oxide trihydrate ($K_2SnO_3{\cdot}3H_2O$, 99.5%), Potassium hydroxide (KOH, 95%) and urea (≥99.5%) and were purchased from Aladdin Bio-Chem Technology Co. Commercial PAN-based graphite felt (GF, 5 mm thickness) was purchased from Gansu HaoShi Carbon Fiber Co., Ltd.), Nafion 117 membrane was purchased from DuPont.

Pretreatment of Materials: The GF was calcined in a muffle furnace at 400 °C for 2 h with a heating rate of 5 °C min^{-1} to improve the hydrophilic properties, labeled as TGF. For membrane pretreatment, the as-received membrane was first treated in 5% H_2O_2 under 60 °C for 1 h to remove impurities and then transferred to 5% H_2SO_4 under 60 °C for 1 h. Second, the membrane was treated in 1 M KOH under 60 °C for 2 h to change H- to K-type. The membrane was washed by DI water after each step to remove the chemicals and impurities.

Material Characterization: The morphologies of samples were characterized using a scanning electron microscope (SEM) equipped with X-ray mapping (FEI QUANTA 600 FE-SEM, 10 kV). The crystalline structure of the GF samples was characterized by X-ray diffraction (XRD, D2 PHASER XE-T X-ray diffractometer System) in the range of 10° and 80°. X-ray photoelectron spectroscopy (XPS) was conducted on a Thermo Scientific K-Alpha$^+$ spectrometer equipped with a monochromatic Al Kα X-ray source (1486.6 eV) operating at 100 W. The optical observation of Sn deposition was carried out by optical microscope (Microscope Axio Imager.A2m).

Electrochemical Characterization: The cyclic voltammetry (CV) was measured using a conventional three-electrode cell system by an

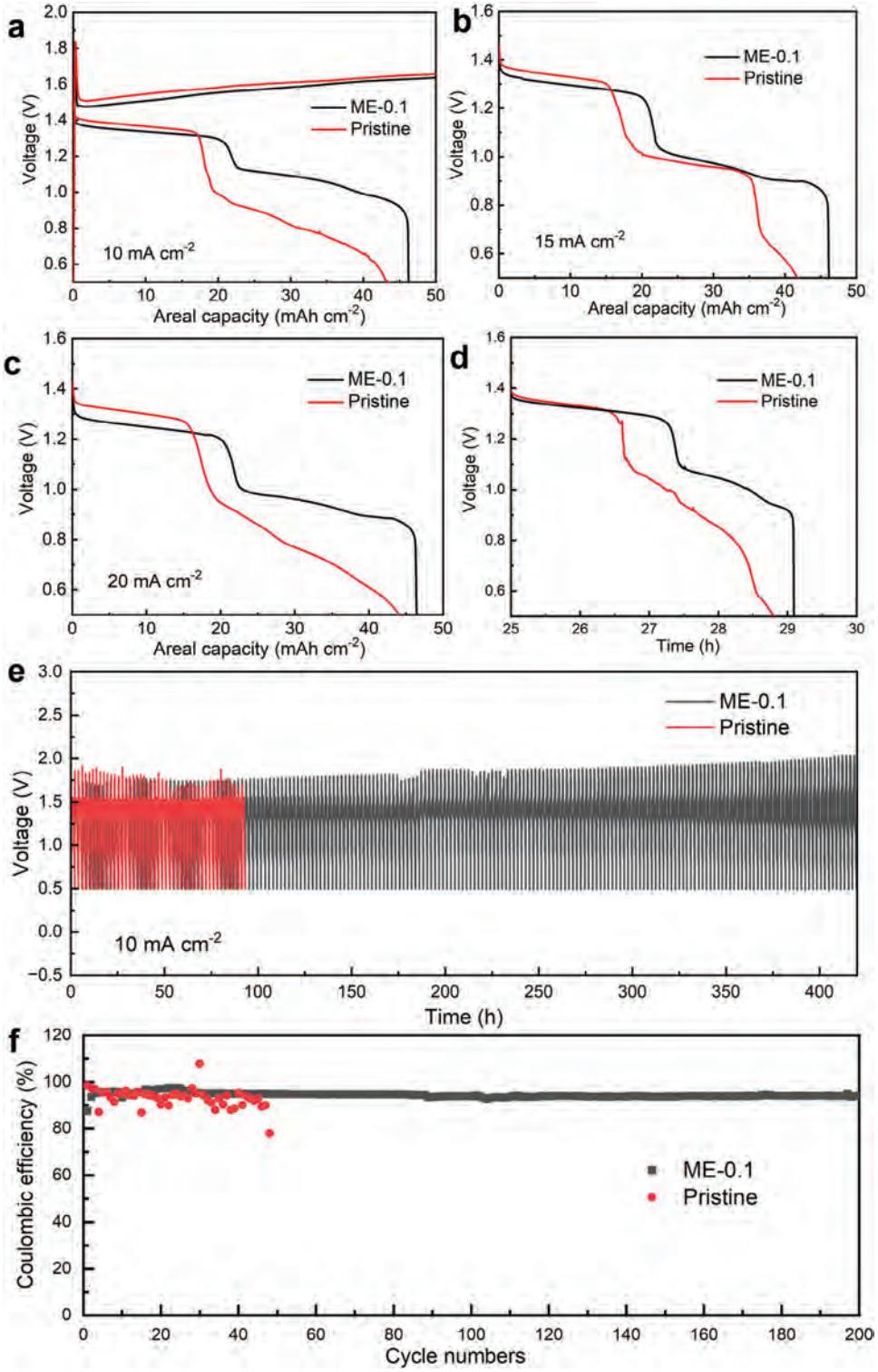

Figure 6. Galvanostatic charge/discharge curves of Sn-I full cells in the pristine electrolyte and ME-0.1 at a) 10 mA cm^{-2}; discharge curves at b) 15 mA cm^{-2} and c) 20 mA cm^{-2}; d) Discharge curves of Sn-I full cell after 5 h charging and 20 h idle period; e) Galvanostatic voltage profiles and f) Coulombic efficiency of Sn-I full cell at a current density of 10 mA cm^{-2} and capacity of 10 mAh cm^{-2}.

Table 1. Areal capacity and average discharge voltage of Sn-I full cell.

Current density (mA cm^{-2})	10		15		20	
Negolyte	Pristine	ME-0.1	Pristine	ME-0.1	Pristine	ME-0.1
Areal capacity (mAh cm^{-2})	43.5	46.2	41.7	46.1	44.1	45.7
Average discharge voltage (V)	1.05	1.18	1.07	1.11	0.98	1.08

electrochemical workstation (ZAHNER-Elektrik, Germany) at room temperature (20 °C). The saturated calomel electrode (Hg/Hg_2Cl_2/KCl, 0.241 V vs SHE) and a platinum gauze were used as the reference electrode and counter electrode, respectively, and TGF was employed as the working electrode.

Flow Battery Assembly: 1.5 M $K_2SnO_3{\cdot}3H_2O$ +1 M KOH was used as negolyte, and excessive 4 M KI solution was used as posolyte. For negolyte modification, urea was employed as an additive using various concentrations (0.05, 0.1, and 0.2 M) for the concentration optimization. The modified electrolyte is denoted ME-X (X = 0.05, 0.1, 0.2 M urea). The flow battery with a geometric electrode area (3 × 3 cm^2) for each half-cell was used to evaluate the performance of Sn-I full cell, the compression ratio of TGF was 25%. The posolyte flow rate was 45 mL min^{-1}, and negolyte flow rate was 30 mL min^{-1}. The charge/discharge experiments were carried out at a constant current density within a potential window of 0.5–1.7 V. The safe voltage limit for charging is set as 2 V. The rate performance and standby test were measured by an electrochemical workstation (ZAHNER-Elektrik, Germany). The cycling of batteries was studied using a Neware battery test system (Neware, Shenzhen, China) with limited volume of negolyte (15 mL) and without any deep discharge. The flow battery running was conducted at room temperature (20 °C).

Supporting Information

Supporting Information is available from the Wiley Online Library or from the author.

Acknowledgements

Y.Y. and Y.X. contributed equally to this work. The study was supported by the Research Grants Council of Hong Kong, the General Research Fund (Grant no. 11308720 and 11306021), and the Innovation and Technology Commission (Grant no. PRP/032/20FX). The authors would like to thank Fei Liu, Yanli Chu, Weilu Li, Xiangkun Bo, Weijun Zhou, and Xiangyang Zhang (Department of Mechanical Engineering, City University of Hong Kong) for their valuable advice.

Conflict of Interest

The authors declare no conflict of interest.

Data Availability Statement

The data that support the findings of this study are available from the corresponding author upon reasonable request.

Keywords

aqueous redox flow battery, Sn deposition, $Sn(OH)_6^{2-}$/Sn redox couple, urea

Received: July 29, 2024
Published online: August 12, 2024

[1] a) A. Khor, P. Leung, M. Mohamed, C. Flox, Q. Xu, L. An, R. Wills, J. Morante, A. A. Shah, *Mater. Today Energy* **2018**, *8*, 80; b) Q. Xu, T. Zhao, *Prog. Energy Combust. Sci.* **2015**, *49*, 40.
[2] a) D. K. Kim, S. J. Yoon, J. Lee, S. Kim, *Appl. Energy* **2018**, *228*, 891; b) T. Li, F. Xing, T. Liu, J. Sun, D. Shi, H. Zhang, X. Li, *Energy Environ. Sci.* **2020**, *13*, 4353.
[3] H. Zhang, *Nature* **2014**, *508*, 319.
[4] a) S. Jin, Y. Shao, X. Gao, P. Chen, J. Zheng, S. Hong, J. Yin, Y. L. Joo, L. A. Archer, *Sci. Adv.* **2022**, *8*, eabq4456; b) X. Xie, F. Mushtaq, Q. Wang, W. A. Daoud, *ACS Energy Lett.* **2022**, *7*, 3484.
[5] a) M. Hu, A. P. Wang, J. Luo, Q. Wei, T. L. Liu, *Adv. Energy Mater.* **2023**, *13*, 2203762; b) J. Yang, H. Yan, H. Hao, Y. Song, Y. Li, Q. Liu, A. Tang, *ACS Energy Lett.* **2022**, *7*, 2331.
[6] Y. Zeng, Z. Yang, F. Lu, Y. Xie, *Appl. Energy* **2019**, *255*, 113756.
[7] Y. Zheng, Á. P. Ramos, H. Wang, G. Álvarez, A. Ridruejo, J. Peng, *Mater. Today Energy* **2023**, *34*, 101286.
[8] a) Z. Yuan, Y. Yin, C. Xie, H. Zhang, Y. Yao, X. Li, *Adv. Mater.* **2019**, *31*, 1902025; b) K. Gong, X. Ma, K. M. Conforti, K. J. Kuttler, J. B. Grunewald, K. L. Yeager, M. Z. Bazant, S. Gu, Y. Yan, *Energy Environ. Sci.* **2015**, *8*, 2941.
[9] W. Xiang, M. Yang, M. Ding, X. Chen, J. Liu, G. Zhou, C. Jia, G. I. N. Waterhouse, *Energy Storage Mater.* **2020**, *61*, 102894.
[10] a) G. Garcia, E. Ventosa, W. Schuhmann, *ACS Appl. Mater. Interfaces* **2017**, *9*, 18691; b) L. Zhi, T. Li, X. Liu, Z. Yuan, X. Li, *Nano Energy* **2022**, *102*, 107697.
[11] C. House, G. Kelsall, *Electrochim. Acta* **1984**, *29*, 1459.
[12] Y. Yao, Z. Wang, Z. Li, Y. C. Lu, *Adv. Mater.* **2021**, *33*, 2008095.
[13] R. Tran, Z. Xu, B. Radhakrishnan, D. Winston, W. Sun, K. A. Persson, S. P. Ong, *Sci. Data* **2016**, *3*, 160080.
[14] A. Sharma, Y. Jang, J. Jung, *Surf. Eng.* **2015**, *31*, 458.
[15] X. Deng, M. Koopman, N. Chawla, K. Chawla, *Mater. Sci. Eng., A* **2004**, *364*, 240.
[16] Y. Yin, S. Wang, Q. Zhang, Y. Song, N. Chang, Y. Pan, H. Zhang, X. Li, *Adv. Mater.* **2020**, *32*, 1906803.
[17] a) J.-H. Lee, R. Kim, S. Kim, J. Heo, H. Kwon, J. H. Yang, H.-T. Kim, *Energy Environ. Sci.* **2020**, *13*, 2839; b) S. Bae, J. Lee, D. S. Kim, *J. Power Sources* **2019**, *413*, 167; c) J. Wu, Q. Dai, H. Zhang, X. Li, *Energy Storage Mater.* **2021**, *35*, 687.
[18] a) M. Kim, D. Yun, J. Jeon, *J. Power Sources* **2019**, *438*, 227020; b) Q. Jian, M. Wu, H. Jiang, Y. Lin, T. Zhao, *J. Power Sources* **2021**, *484*, 229238; c) W. Xu, K. Zhao, W. Huo, Y. Wang, G. Yao, X. Gu, H. Cheng, L. Mai, C. Hu, X. Wang, *Nano Energy* **2019**, *62*, 275.
[19] D. W. Oxtoby, *Acc. Chem. Res.* **1998**, *31*, 91.
[20] Z. Zhang, M. G. Lagally, *Science* **1997**, *276*, 377.
[21] F. Wang, J. Xie, D. Zheng, F. Yang, H. Zhang, X. Lu, *Adv. Mater.* **2022**, *34*, 2200085.
[22] G. Wang, J. Chen, X. Wang, J. Tian, H. Kang, X. Zhu, Y. Zhang, X. Liu, R. Wang, *J. Energy Chem.* **2014**, *23*, 73.
[23] a) Y. Yang, K. Li, Y. Meng, Y. Wang, Z. Wu, *New J. Chem.* **2018**, *42*, 6873; b) Y. Yang, C. Yin, K. Li, H. Tang, Y. Wang, Z. Wu, *J. Electrochem. Soc.* **2019**, *166*, F755.
[24] Y. Yang, Y. Zhao, R. Zhang, *J. Mater. Chem. A* **2024**, *12*, 375.